Cancer Cell
Article

Identification of the JNK Signaling Pathway as a Functional Target of the Tumor Suppressor PTEN

Igor Vivanco,[1] Nicolaos Palaskas,[2] Chris Tran,[3] Stephen P. Finn,[5] Gad Getz,[4] Norman J. Kennedy,[7] Jing Jiao,[2] Joshua Rose,[5] Wanling Xie,[6] Massimo Loda,[5] Todd Golub,[4,5] Ingo K. Mellinghoff,[2] Roger J. Davis,[7,8] Hong Wu,[2] and Charles L. Sawyers[3,*]
[1] Molecular Biology Institute
[2] Department of Molecular and Medical Pharmacology
University of California at Los Angeles, Los Angeles, CA 90095, USA
[3] Human Oncology and Pathogenesis Program, Memorial Sloan-Kettering Cancer Center, 1275 York Avenue, New York, NY 10021, USA
[4] Broad Institute of Harvard and the Massachusetts Institute of Technology, 320 Charles Street, Cambridge, MA 02141, USA
[5] Department of Medical Oncology
[6] Department of Biostatistics and Computational Biology
Dana-Farber Cancer Institute, Harvard Medical School, 44 Binney Street, Boston, MA 02115, USA
[7] Program in Molecular Medicine
[8] Howard Hughes Medical Institute
University of Massachusetts, Worcester, MA 01605, USA
*Correspondence: sawyersc@mskcc.org
DOI 10.1016/j.ccr.2007.04.021

SUMMARY

Although most oncogenic phenotypes of *PTEN* loss are attributed to AKT activation, AKT alone is not sufficient to induce all of the biological activities associated with PTEN inactivation. We searched for additional PTEN-regulated pathways through gene set enrichment analysis (GSEA) and identified genes associated with JNK activation. *PTEN* null cells exhibit higher JNK activity, and genetic studies demonstrate that JNK functions parallel to and independently of AKT. Furthermore, *PTEN* deficiency sensitizes cells to JNK inhibition and negative feedback regulation of PI3K was impaired in *PTEN* null cells. Akt and JNK activation are highly correlated in human prostate cancer. These findings implicate JNK in PI3K-driven cancers and demonstrate the utility of GSEA to identify functional pathways using genetically defined systems.

INTRODUCTION

Inactivation of the tumor suppressor *PTEN* is among the most common genetic lesions in human cancer. PTEN functions as a tumor suppressor by dephosphorylating the lipid products of PI3K, thus limiting the intracellular pool of these second messengers and attenuating downstream signaling. Loss of PTEN causes an increase in intracellular PIP3 levels and activation of PH-domain-containing molecules such as AKT. AKT phosphorylates substrates involved in mediating survival from apoptosis, proliferation, angiogenesis, and the regulation of glucose metabolism (Vivanco and Sawyers, 2002).

The serine/threonine kinase mTOR is an effector of AKT. AKT derepresses mTOR activity by phosphorylating TSC2 (Inoki et al., 2002), a negative regulator of mTOR function.

SIGNIFICANCE

PTEN is the second most commonly mutated tumor suppressor in human cancers. We searched for pathways deregulated by *PTEN* inactivation using isogenic pairs of PTEN wild-type and PTEN knockdown cell lines and gene set enrichment analysis. The JNK pathway was significantly associated with PTEN loss and chosen for validation. We confirmed biochemical activation of JNK in PTEN-deficient cells and found that *PTEN* inactivation increases sensitivity to JNK inhibition in a synthetic lethal-like fashion. Concurrent activation of AKT and JNK synergized in transformation assays. Interestingly, *PTEN* null cells have a defect in IRS-1-regulated feedback inhibition of PI3K that permits chronic activation of the pathway. These results implicate JNK as a critical component of the PTEN/PI3K pathway and a potential therapeutic target.

Tumors with *PTEN* mutations are sensitized to the growth-suppressive action of mTOR inhibitors, indicating that *PTEN* null cancers become dependent on mTOR-driven signals (Neshat et al., 2001; Podsypanina et al., 2001; Wendel et al., 2004; Yilmaz et al., 2006). Understanding the molecular pathways downstream of PTEN may identify additional targets for the treatment of tumors with dysregulated PI3K function.

Although AKT explains many of the phenotypes associated with PTEN inactivation, the biological consequences of *PTEN* gene targeting and genetic activation of *AKT* are not completely overlapping. Mice with prostate-specific PTEN inactivation develop invasive carcinoma with complete penetrance (Trotman et al., 2003; Wang et al., 2003). In contrast, transgenic mice carrying an activated allele of *AKT* under the regulation of a prostate-specific promoter develop prostate intraepithelial neoplasia (PIN) but did not progress to cancer (Majumder et al., 2003). These data as well as findings from other models raise the possibility that additional pathways downstream from PI3K can complement AKT in tumorigenesis caused by *PTEN* loss. For example, in an in vitro model of breast cancer that relies on concurrent expression of hTERT, SV40 large T antigen, and activated PI3K for transformation, activated alleles of *AKT* and *RAC1* can replace PI3K (Zhao et al., 2003), suggesting that these two signals may contain most (if not all) of the oncogenic signals transduced by PI3K.

Several groups have reported transcriptional signatures of PTEN, typically through reconstitution experiments in PTEN-deficient tumor cells (Hong et al., 2000; Li et al., 2006; Musatov et al., 2004; Simpson et al., 2001; Stolarov et al., 2001). While useful, this approach does not reflect the physiologic situation in tumors where PTEN expression is lost rather than restored. Here, we conducted such experiments using isogenic tumor cell line pairs in which *PTEN* inactivation was engineered through RNA interference. We also used the analytical method known as gene set enrichment analysis (GSEA) (Subramanian et al., 2005) to search for pathways dysregulated as a consequence of PTEN loss, as this approach can offer advantages over traditional analytical methods in identifying coordinately regulated gene sets versus differences in expression of single genes (Majumder et al., 2004; Monti et al., 2005; Mootha et al., 2003).

Among the gene sets that were consistently enriched in PTEN-deficient samples was the Jun N-terminal Kinase (JNK) pathway, which attracted our attention due to opportunities for pharmacological intervention. We confirmed functional upregulation of the pathway in *Pten* knockout (KO) mouse embryonic fibroblasts (MEF). We also found the increase in Jnk activity was independent of Akt activation. In addition, AKT and JNK synergized in transformation assays, both in vitro and in vivo, further suggesting that AKT and JNK function in parallel rather than in a linear pathway. Conversely, both Jnk inhibition (specifically JNK1) and *JunD* inactivation selectively inhibited the growth of *Pten* null cells. Finally, we found *PTEN* null cells maintain constitutive activation of the PI3K pathway, in part, through loss of an IRS1-mediated feedback loop. Our findings implicate JNK and AKT as complementary signals in PIP3-driven tumorigenesis and suggest that JNK may be a therapeutic target in *PTEN* null tumors.

RESULTS

PTEN Loss Enhances Expression of Genes in the JNK Pathway

Although much is known about the contribution of AKT to PI3K-driven tumorigenesis, the identity and biological relevance of AKT-independent pathways downstream of PI3K are relatively unexplored. To identify additional pathways that may participate in tumorigenesis caused by *PTEN* loss, we took an unbiased approach to look for gene sets that were enriched in PTEN-deficient cells. We first generated a series of human isogenic cell line pairs in which PTEN was knocked down by RNA interference. We derived stable lines of A431 (epidermoid carcinoma), HCC827 (non-small-cell lung carcinoma), and SKBR-3 (mammary adenocarcinoma) cells retrovirally transduced with a small hairpin RNA (shRNA) targeting *PTEN*. These lines were chosen to sample *PTEN* inactivation in several tissue types reflective of the human cancers with *PTEN* loss. PTEN expression was reduced by approximately 90% at the protein level (Figure 1A).

We used GSEA to identify gene sets enriched in each of the three PTEN-deficient sublines (hereafter referred to as PR for PTEN RNAi) compared to their parental counterparts. Thirty-six gene sets were enriched in each of the three individual cell line pairs (Figure 1B, Venn diagram) and presumably reflect "consensus" pathways deregulated by PTEN loss irrespective of tissue specificity and genetic background. Thirty-four of these 36 commonly enriched gene sets were also identified through a related analysis strategy where all three PTEN-positive cell lines were pooled into a single class and compared to the pooled PR sublines (Figure 1C). Among these 34 gene sets, the JNK pathway (see Figure S1A for enrichment data in the Supplemental Data available with this article online) was of particular interest because JNK is essential for oncogene-driven transformation in certain contexts (Hess et al., 2002; Rodrigues et al., 1997) and is amenable to targeting by small molecule kinase inhibitors (Manning and Davis, 2003). Upon closer inspection of the mRNAs included into the *JNK* pathway gene set, we noted that three JNK phosphatases (*DUSP4*, *DUSP8*, and *DUSP10*) were included with ~20 *JNK* pathway kinases, adaptors, and downstream transcription factor targets such as *JUN* and *ATF2* (Table S1). Since the kinases and phosphatases presumably function in an opposing fashion, we removed the three *JNK* phosphatases from the original *JNK* pathway gene set and repeated the GSEA. The curated *JNK* gene set (excluding phosphatases) was again enriched in the pooled PTEN null cells and with even greater statistical significance than the original gene set (higher normalized enrichment score and lower p value) (Figure 1C, bottom). The *JNK* phosphatase gene

A

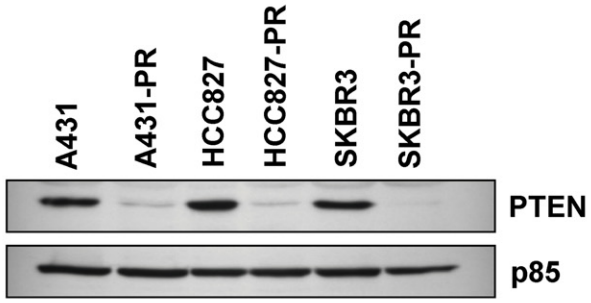

B

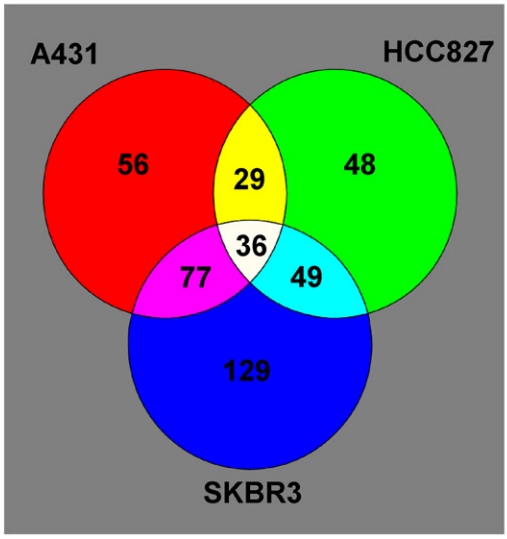

C

GENE SETS ENRICHED IN "PR" SUBLINES	A431		HCC827		SKBR3		POOLED LINES	
	NES	p VALUE	NES	p VALUE	NES	p VALUE	NES	p VALUE
pparPathway	1.755	0.010	0.806	0.699	1.356	0.132	2.032	0.004
vobesityPathway	1.527	0.066	0.856	0.623	1.955	0.004	1.762	0.016
FA	1.669	0.026	0.684	0.859	1.109	0.322	1.728	0.030
pmlPathway	1.555	0.051	1.037	0.411	1.036	0.378	1.695	0.029
ccr5Pathway	1.019	0.411	0.811	0.711	1.308	0.164	1.640	0.027
shh_lisa	0.894	0.597	1.006	0.435	0.807	0.727	1.616	0.028
HUMAN_CD34_ENRICHED_TF_JP	1.229	0.182	0.879	0.612	1.132	0.313	1.551	0.060
cacamPathway	1.499	0.056	0.956	0.528	0.932	0.536	1.502	0.063
dreamPathway	0.919	0.532	1.485	0.081	1.078	0.348	1.386	0.107
ST_JNK_MAPK_Pathway	1.380	0.107	0.988	0.447	1.011	0.426	1.375	0.123
ST_GRANULE_CELL_SURVIVAL_PATHWAY	0.830	0.665	1.134	0.295	1.221	0.224	1.373	0.120
betaoxidationPathway	1.362	0.126	0.668	0.873	0.736	0.787	1.301	0.174
cremPathway	0.736	0.770	0.835	0.651	0.993	0.466	1.247	0.207
ppargPathway	1.600	0.039	0.939	0.508	0.589	0.936	1.239	0.205
etsPathway	0.519	0.988	1.347	0.138	1.014	0.401	1.229	0.204
41bbPathway	0.743	0.779	0.832	0.656	1.340	0.139	1.226	0.213
carm-erPathway	0.583	0.955	1.201	0.217	0.858	0.660	1.224	0.217
SIG_Regulation_of_the_actin_cytoskeleton_by_Rho_GTPases	1.018	0.412	0.534	0.985	0.941	0.494	1.152	0.262
ST_Differentiation_Pathway_in_PC12_Cells	0.697	0.805	1.387	0.112	1.076	0.341	1.096	0.329
arenrf2Pathway	0.712	0.825	0.578	0.960	1.327	0.153	1.076	0.361
huntingtonPathway	0.842	0.658	0.560	0.965	1.808	0.017	1.070	0.349
keratinocytePathway	0.793	0.709	1.015	0.409	1.142	0.294	1.061	0.379
RAR_UP	0.699	0.856	1.021	0.425	0.693	0.873	0.988	0.462
MAP00512_O_Glycans_biosynthesis	0.805	0.722	0.933	0.504	0.749	0.779	0.983	0.463
pelp1Pathway	0.971	0.496	0.903	0.587	0.973	0.466	0.959	0.512
SA_MMP_CYTOKINE_CONNECTION	1.428	0.106	0.764	0.746	1.496	0.060	0.958	0.486
TESTIS_GENES_FROM_XHX_AND_NETAFFX	0.749	0.808	1.012	0.401	1.101	0.345	0.938	0.528
ST_Ga12_Pathway	0.777	0.749	0.857	0.617	0.791	0.739	0.924	0.543
tnfr1Pathway	1.234	0.205	0.891	0.595	0.901	0.564	0.861	0.654
tertPathway	1.014	0.430	0.881	0.591	1.027	0.431	0.812	0.693
akap96Pathway	1.123	0.293	0.961	0.487	1.355	0.118	0.801	0.717
NFKB_REDUCED	1.314	0.157	0.750	0.800	0.945	0.510	0.646	0.895
plcePathway	0.741	0.788	0.843	0.666	0.872	0.604	0.638	0.895
ecmPathway	0.814	0.677	1.309	0.136	0.454	0.994	0.559	0.967

GENE SETS ENRICHED IN "PR" SUBLINES	A431		HCC827		SKBR3		POOLED LINES	
	NES	p VALUE	NES	p VALUE	NES	p VALUE	NES	p VALUE
ST_JNK_MAPK-Pathway (excluding JNK Phosphatases)	1.593	0.049	0.988	0.453	1.101	0.321	1.603	0.044
JNK Phosphatases (DUSP4, DUSP8, DUSP10)	-1.686	0.015	-1.073	0.363	-0.921	0.508	-1.126	0.313

Figure 1. PTEN Inactivation Leads to Enrichment of a Small Number of Gene Sets

(A) RNAi-mediated inactivation of PTEN was confirmed by western blot in the indicated cell lines (the suffix -PR indicates PTEN RNAi). Immunoblot analysis using a p85 antibody was also carried out as a loading control.

(B) Venn diagram of three different GSEA analyses run on the three parental and -PR tumor line pairs. The number of gene sets associated with PTEN loss and the overlap between cell line pairs is shown.

(C) List of the top 36 genes sets enriched in all three cell line pairs. The *JNK* pathway gene set is highlighted in yellow. The table at the bottom shows the repeat GSEA when the three JNK phosphatases were removed from the curated *JNK* pathway gene set (see also Table S1). (NES, normalized enrichment score).

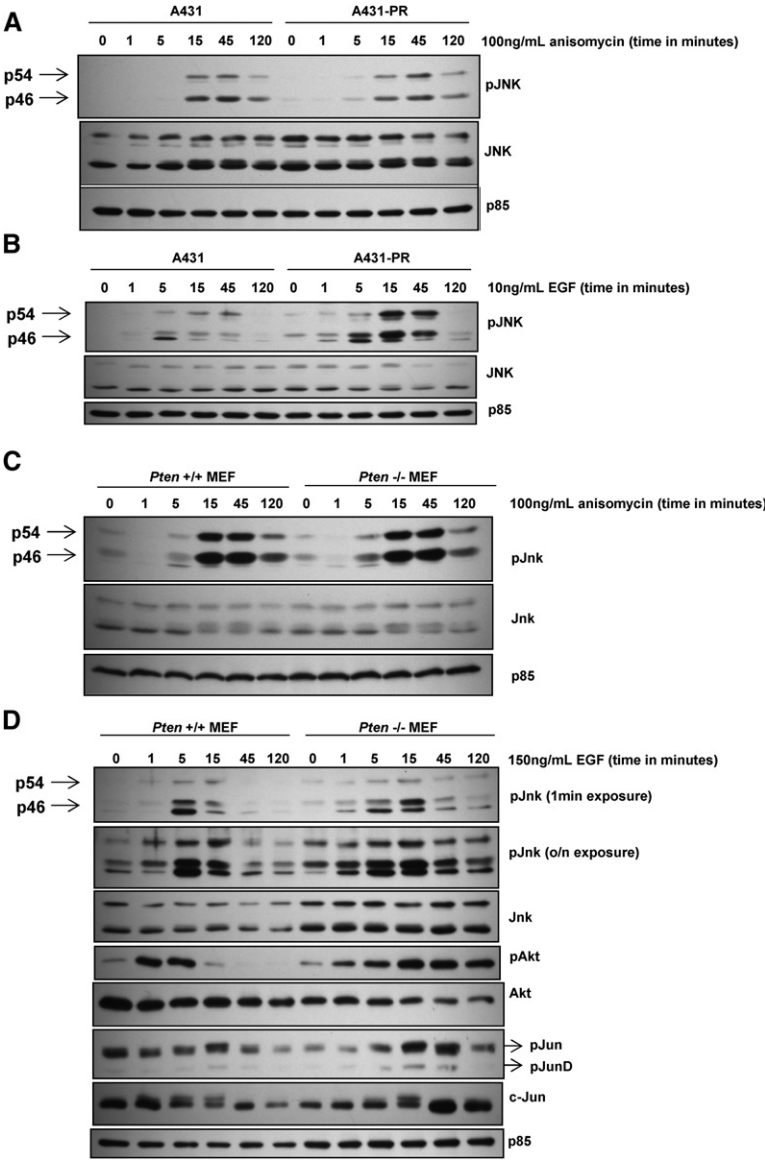

Figure 2. The JNK Pathway Is Activated as a Result of PTEN Loss

(A) Exponentially growing A431 and A431-PR cells were treated with 100 ng/ml anisomycin. At the indicated times, cells were lysed and the lysates were normalized and subjected to immunoblot using the indicated antibodies.

(B) A431 and A431-PR cells were serum starved for 48 hr and subsequently challenged with 10 ng/ml EGF. At the indicated times, cells were lysed and the lysates were normalized and subjected to immunoblot using the indicated antibodies.

(C) Exponentially growing $Pten^{+/+}$ and $Pten^{-/-}$ MEFs were treated with 100 ng/ml anisomycin. At the indicated times, cells were lysed and the lysates were normalized and subjected to immunoblot using the indicated antibodies.

(D) $Pten^{+/+}$ and $Pten^{-/-}$ MEFs were serum starved for 24 hr and subsequently challenged with 150 ng/ml EGF. At the indicated times, cells were lysed and the lysates were normalized and subjected to immunoblot using the indicated antibodies.

set was negatively enriched (bottom table in Figure 1C and Figure S1B), providing further confidence in the PTEN loss/JNK pathway association.

PTEN Loss Leads to Enhanced JNK Activation

To biochemically evaluate the GSEA-predicted consequences of PTEN loss on JNK function, we measured growth factor- and chemical stress-induced JNK activation in A431 and A431-PR cells using activation-state-specific antibodies against JNK. While both cell lines showed identical JNK activation profiles in response to anisomycin (Figure 2A), EGF-induced JNK activation was higher and persisted longer in PTEN-deficient cells (Figure 2B). We observed a similar pattern of Jnk activation in MEFs carrying a "floxed" *Pten* allele (Freeman et al., 2003) deleted by retroviral delivery of Cre recombinase (Figures 2C and 2D) and when fetal bovine serum (FBS) rather than EGF was used as the activation stimulus in both MEFs and A431 cells (Figure S2 and data not shown).

In addition to growth factor-induced Jnk activity, steady-state Jnk activity was higher in *Pten* null MEFs, albeit at more modest levels. Phospho-Jnk levels were consistently elevated in $Pten^{-/-}$ MEFs (Figure S3A), and this increase was confirmed by in-gel kinase assays (Figure S3B). Of note, the magnitude of Jnk1 activation (approximately 2-fold higher in *Pten*-deficient cells) was greater than Jnk2 (approximately 50% increase). Phosphorylation levels of the Jnk substrate c-Jun were also higher in $Pten^{-/-}$ MEFs (Figure S3A). JunD phosphorylation, recognized by the same phospho-c-Jun antibody as a faster migrating band, was increased as well (best seen in Figures 2D, 5B, and 6C). Levels of both phospho-c-Jun and phosphoS6 (a downstream readout of Akt) were also higher in $Pten^{-/-}$ brain lysates, derived

from a floxed *Pten/Nestin-Cre* mouse cross (Groszer et al., 2006) (Figure S3C). In a reciprocal set of experiments, ecdyson-induced PTEN expression in the *PTEN* null glioma cell line U87 (Stolarov et al., 2001) repressed JNK and AKT activity (Figure S3D).

The Increase in JNK Activity Elicited by PTEN Loss Occurs Through Multiple Mechanisms

Previous reports have shown that a constitutively active *PI3K* allele is sufficient to activate JNK (Klippel et al., 1996); therefore, we suspected that Jnk activation in *Pten* null cells would also be Pi3k-dependent. The Pi3k inhibitor LY294002 inhibited Jnk activation in *Pten* null MEFs and in a prostate cancer cell line derived from *Pten* knockout mice (PTEN-CaP8) in a dose-dependent fashion, but to a much lesser degree in wild-type MEFs or in a *Pten* wild-type prostate cancer cell line derived from large T antigen transgenic mice (TRAMP-C1) (Foster et al., 1997)(Figures 3A and 3B). Similar findings were observed using a Jun reporter assay, where the increased Jnk activity seen in $Pten^{-/-}$ MEFs was restored to the baseline levels seen in $Pten^{+/+}$ MEFs by LY294002 treatment (Figure 3C, red bar). Conversely, Jnk reporter activity was increased in *Pten* wild-type MEFs expressing a constitutively active allele of *Pi3k* (Myr-p110*) but not in *Pten* null MEFS, consistent with the notion that Pi3k activation and Pten inactivation are likely epistatic (Figure 3D).

We next considered the molecular basis of Jnk activation through the Pi3k/Pten pathway. Previously, we reported that *Pten* null MEFs have elevated Cdc42 and Rac1 catalytic activity (Liliental et al., 2000). Mixed-lineage kinase-3 (Mlk3) is a Jnk kinase kinase downstream of Rac1, and the *Drosophila* Mlk3 homolog Slipper was one of several genes isolated in a suppressor screen of the Pten knockdown phenotype in flies (Kiger et al., 2003). Therefore, we asked if the elevated Jnk activity in *Pten* null cells is dependent on Mlk3 and Rac1. In the c-*jun* reporter assay, dominant negative MLK3 selectively repressed Jnk activity in $Pten^{-/-}$ MEFs (Figure 3C, light green bar). Jnk activity was also suppressed by a dominant negative allele of RAC1 but with less specificity for *Pten* null MEFs than seen with Mlk3 (Figure 3C, yellow bar).

Based on our GSEA analysis, we suspected that PTEN might also regulate JNK through its effects on transcription. To address this possibility, we repeated the EGF induction experiments described above in the presence of the transcriptional inhibitor actinomycin-D (ActD). Peak JNK activation (reached after 15 min of EGF stimulation) was unaffected by ActD; however, the extended longevity of the signal seen at 120 min in PTEN-deficient cells was reversed (Figure 3E). In fact, JNK phosphorylation dropped below basal levels at this time point (Figure 3E, compare the 0 and 120 min time points in A431-PR cells). Taken together, these data implicate at least two mechanisms by which PTEN loss affects JNK activity. Increased PIP_3 levels are most likely responsible for the higher peak level of growth factor-induced JNK activation in *PTEN* null cells, whereas the increased duration of JNK activation is transcription-dependent.

PTEN Loss Sensitizes Cells to JNK Pathway Inhibition

To investigate the biological importance of Jnk deregulation by *Pten* loss, we studied the effects of Jnk pathway inhibition on cell growth. Using the isogenic MEF model, we acutely infected cells with retroviral shRNAs targeting either *Jnk1* or *Jnk2* (Figure 4A, right panel) or the Jnk transcription factor target JunD (Figure 4B, right panel). JunD was chosen because (1) it transduces Jnk survival signals (Lamb et al., 2003), (2) it promotes (rather than suppresses) growth when the tumor suppressor MEN1 is inactivated (Agarwal et al., 2003) (and might function similarly with Pten) and (3) pJunD levels are increased in *Pten* null MEFs. Both Jnk1 and JunD knockdown selectively inhibited the growth of *Pten* null MEFs by about 50 percent (Figures 4A and 4B, left panels). JunD knockdown in wild-type MEFs caused a modest increase in proliferation, consistent with the tumor suppressor function of JunD in certain contexts (Pfarr et al., 1994). *Jnk1* RNAi was similarly effective in selectively blocking the growth of *Pten* null (PTEN-CaP8), but not Pten-positive (TRAMP-C1), prostate cancer cells (Figure 4C). In contrast to Jnk1, the antiproliferative effects of Jnk2 knockdown were seen regardless of *Pten* background (Figure 4A, left panel, yellow bars), in agreement with previous work showing that *JNK2* but not *JNK1* antisense oligonucleotides have broad antiproliferative activity (Du et al., 2004).

We also examined the effects of a relatively selective pyridinylamide JNK inhibitor (hereafter referred to as JNKi) (Szczepankiewicz et al., 2006) in the isogenic *Pten* MEFs. Similar to the Jnk1 and JunD knockdown studies, JNKi blocked the growth of *Pten* null MEFs without affecting wild-type MEFs (Figure 4D, left panel) at concentrations that reduced c-Jun phosphorylation to comparable levels in both lines (Figure 4D, right panels). Total c-Jun levels were lower in JNKi-treated cells as expected since c-Jun expression is positively regulated by its own activity (Angel et al., 1988) (Figure 4D, right panel and Figure S4A). We observed similar results with the widely used but less specific anthrapyrazolone JNK inhibitor SP600125 (Figures S4B and S4C). The collective data from these and the RNA interference experiments indicate that *Pten* null cells acquire dependence on sustained Jnk activation.

In addition to its role in mediating proapoptotic signals (Davis, 2000), Jnk is required for malignant transformation in certain contexts, such as by the *BCR-ABL* leukemia oncogene (Dickens et al., 1997; Hess et al., 2002; Raitano et al., 1995; Rodrigues et al., 1997). To determine if the antiproliferative effects of Jnk1 inhibition observed in vitro extended to tumor models, we assessed the impact of Jnk1 knockdown on tumorigenicity. Retroviral delivery of *Jnk1* shRNA into *Pten* null MEFs almost completely inhibited subcutaneous tumor formation in SCID mice (Figure 4E). Similarly, Jnk1 knockdown (Figure 4F) reduced tumorigenicity of PTEN-CaP8 by 50 percent (Figure 4G). Conversely, *Jnk1* shRNA did not substantially affect tumor incidence in TRAMP-C1 cells, albeit with less-efficient Jnk1 knockdown than in PTEN-CaP8 cells

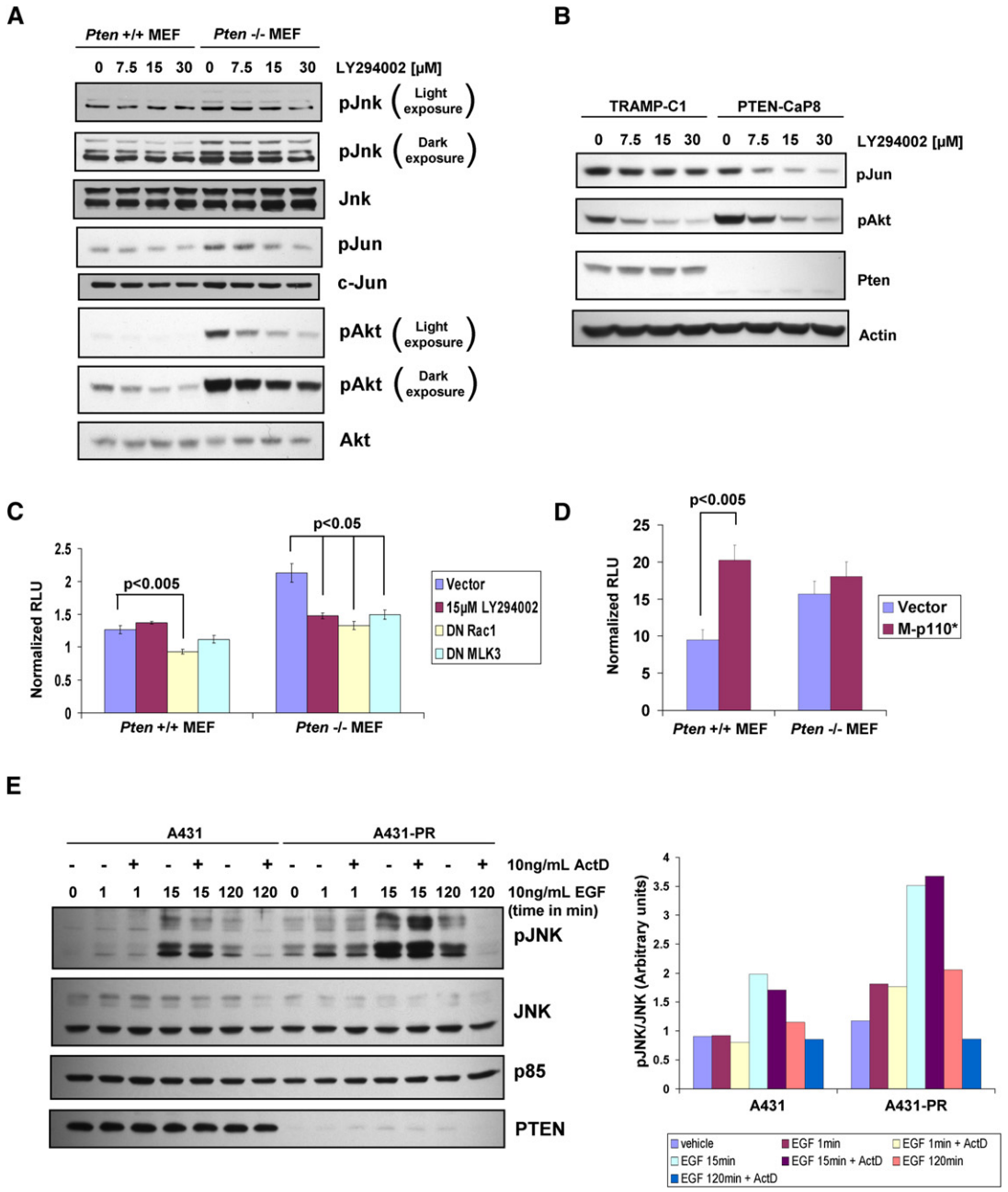

Figure 3. PTEN Regulates JNK Function by Multiple Mechanisms

(A and B) *Pten*$^{+/+}$ and *Pten*$^{-/-}$ MEF, or PTEN-CaP8 and TRAMP-C1 cells were treated with the indicated doses of LY294002 for 6 hr and then lysed. Lysates were subjected to immunoblot using activation state-specific antibodies against phospho-Jnk (pJnk), phospho-c-Jun (pJun), and pAkt (pAKT), or antibodies against total Jnk, c-Jun, Akt, actin, and Pten.

(C) *Pten*$^{+/+}$ and *Pten*$^{-/-}$ MEFs were cotransfected with either empty vector, dominant-negative RAC1 (DN Rac) or dominant-negative MLK3 (DN MLK3) constructs along with AP-1 PathDetect plasmids, or were transfected with PathDetect plasmids and treated with 10 μM LY294002. Jnk activity (mean ± SEM, n = 3) was measured by luciferase reporter assay 36 hr after transfection.

(D) *Pten*$^{+/+}$ and *Pten*$^{-/-}$ MEFs were co-transfected with either empty vector or constitutively active PI3K (M-p110*) along with AP-1 PathDetect plasmids. Jnk activity (mean ± SEM, n = 3) was measured as in (C) 36 hr after transfection.

(E) A431 and A431-PR cells were serum starved for 48 hr and pretreated with 10 ng/ml actinomycin D for 15 min. Cells were then kept in Actinomycin D where indicated and stimulated with 10 ng/ml EGF for the indicated times. Cells were lysed and lysates were normalized before subjecting them to immunoblot with the indicated antibodies. pJNK levels were quantified by densitometry and expressed as a ratio of pJNK over total JNK.

(Figures 4F and 4H). The effect of Jnk1 inhibition in these tumorigenicity assays relative to in vitro proliferation rates suggests that Jnk1 may be even more critical for oncogenic growth.

Jnk and Akt Are Activated Independently and Synergize in Transformation Assays

To determine if Jnk and Akt are activated independently by Pi3k or sequentially through a linear signaling pathway, we measured the effect of loss of function of one on the biochemical activity of the other. Dual inactivation of *Jnk1* and *Jnk2* by gene targeting had no effect on insulin-induced Akt activation in MEFs (Figure 5A), providing evidence that Akt is not downstream of Jnk. We conducted the reciprocal experiment, asking whether Jnk was downstream of Akt, by inhibition of Akt using a previously characterized compound that selectively interferes with PH domain/PIP_3 binding (Barnett et al., 2005; Zhao et al., 2005). Jun phosphorylation was unaffected by doses that clearly lowered Akt and S6 phosphorylation (Figure 5B). These results suggest that Akt and Jnk are independently activated by Pi3k through parallel pathways rather than in sequence. One prediction is that constitutive activation of both Jnk and Akt should give a greater biological effect than individual activation of each signal. To test this hypothesis, we expressed activated *AKT* and activated *JNK* separately or simultaneously in NIH3T3 cells by retroviral infection and compared growth rates in soft agar and in mice. Constitutive JNK activation was achieved using a modified version of a previously characterized MKK7/JNK1 fusion protein (Lei et al., 2002) (hereafter called JNK*), where phosphomimetic mutations (Wolter et al., 2002) were introduced in the *MKK7* moiety to achieve maximal activation. Neither AKT nor JNK was sufficient to induce anchorage-independent growth, whereas the combination clearly was (Figure 5C, left panel). Furthermore, the growth of these doubly transduced colonies, upon replating in soft agar after brief propagation in vitro, was completely inhibited by SP600125 treatment (Figure 5C, right panel). Similarly, doubly transduced NIH3T3 cells formed larger tumors more quickly after subcutaneous implantation in SCID mice (Figure 5D) and grew more quickly in liquid culture (Figure S5).

Because *PTEN* loss is common in glioma (Wang et al., 1997) and JNK activity is elevated in some of these tumors (Antonyak et al., 2002), we extended our findings to an immortalized human astrocyte model of human glioma (NHA) (Sonoda et al., 2001). As with NIH3T3 cells, only astrocytes expressing both transgenes formed colonies in soft agar (Figure 5E), and doubly transduced astrocytes generated tumors in animals more quickly and with higher penetrance than astrocytes expressing AKT alone (Figure 5F). JNK*-expressing and vector control astrocytes did not form tumors. Collectively, these biochemical and biological studies support a model whereby JNK functions in parallel with AKT to promote tumorigenesis and are consistent with an earlier report that RAC1 (presumably acting upstream of JNK) and AKT could replace PI3K in a breast cancer transformation model (Zhao et al., 2003).

Pten Null Cells Have an Impaired Negative Feedback Loop, Leading to Prolonged Pi3k Activation

Although PI3K pathway signaling is primarily regulated by PTEN, there has been much recent interest in two negative feedback loops, involving S6 kinase and JNK, respectively, that attenuate insulin-induced PI3K activation by phosphorylating insulin receptor substrate (IRS) proteins at serine residues leading to their inactivation (Fujishiro et al., 2003; Gual et al., 2005; Lee et al., 2003). JNK1 appears to be the most relevant JNK isoform in mediating feedback because *JNK1*-deficient (but not JNK2-deficient) mice are protected from diet-induced insulin resistance (Hirosumi et al., 2002). One prediction of our dual AKT/JNK pathway activation model is that both negative feedback loops would be active; therefore, cells should be unable to sustain PI3K activity. Yet, PTEN-deficient tumors have constitutively increased PI3K signaling, suggesting they may be resistant to negative feedback (Figure 6A).

To address this apparent paradox, we first used the mTOR inhibitor rapamycin, which blocks S6 kinase-mediated negative feedback (Easton et al., 2006; O'Reilly et al., 2006; Shi et al., 2005). Wild-type MEFs treated with rapamycin showed a dose-dependent increase in the steady state levels of phospho-Akt (as expected [O'Reilly et al., 2006; Sun et al., 2005]), but *Pten* null MEFs did not, suggesting that negative feedback is impaired in Pten-deficient cells. We observed similar results using the JNK inhibitor: JNKi treatment led to an increase in steady-state pAkt levels in wild-type MEFs but not in *Pten* null MEFs. Therefore, both mTor and Jnk regulate pathway(s) responsible for negative feedback of Akt that is impaired in *Pten* null cells. Similar to pAkt, the steady-state level of Jnk phosphorylation was increased in JNKi-treated cells, indicative of additional negative feedback, but this effect was observed regardless of *Pten* status and therefore suggests a Pi3k-independent negative feedback loop (Figure 6C and Figure S4A).

Since Irs proteins are one target of mTor- and Jnk-dependent negative feedback, we investigated their expression level and phosphorylation status. mRNA (Figure S6) and protein (Figure 6D, left panel) levels of both Irs1 and Irs2 were substantially lower in *Pten* null MEFs. IRS-1 levels were similarly reduced (in cells with detectable basal levels) in the PTEN knockdown tumor sublines used for the GSEA analysis described earlier (Figure 6D, right panel). These findings are consistent with a reciprocal experiment performed by others in which PTEN reconstitution led to an increase in IRS-2 levels (Simpson et al., 2001).

Next, we assessed the impact of Pten loss on insulin-induced Irs-1 phosphorylation and subsequent complex formation with the insulin receptor (Ir-β). LY294002 was used in some experiments as a tool to block downstream signal propagation and thereby eliminate negative feedback. As expected (Haruta et al., 2000), tyrosine

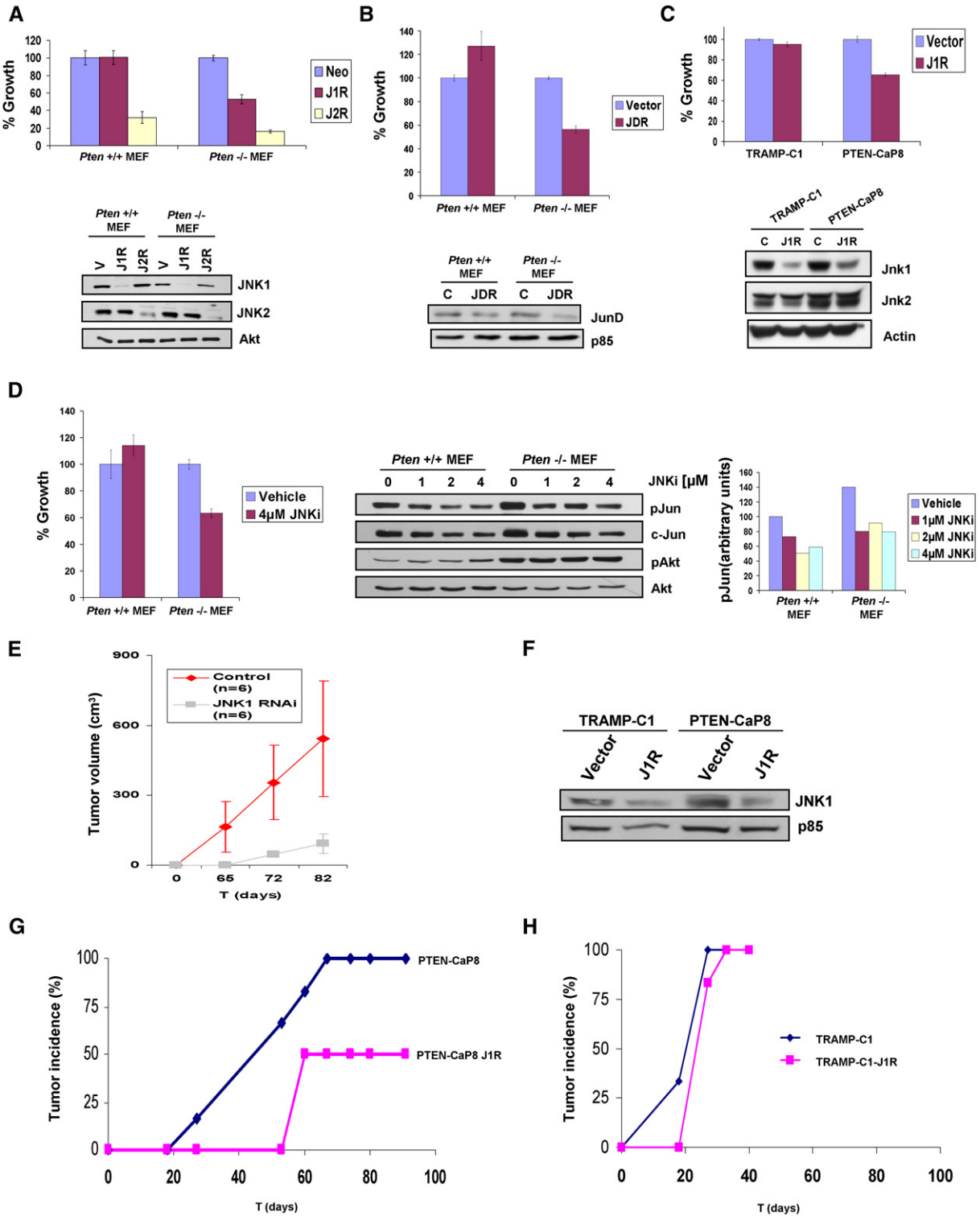

Figure 4. Pten Loss Sensitizes Cells to Jnk Inhibition

(A) *Pten*$^{+/+}$ and *Pten*$^{-/-}$ MEF were retrovirally infected with *Jnk1*-targeted sh*R*NA (J1R) or *Jnk2*-targeted sh*R*NA (J2R). Seventy-two hours after infection, lysates were made and analyzed by immunoblot with the indicated antibodies (bottom). Cells were also seeded and counted the day after seeding and 5 days later. Growth is expressed as the percentage increase in cell number between day 1 and day 5 in relation to vector-infected cells (100% growth) (left, mean ± SEM, n = 3).

phosphorylation of Irs-1 was increased in insulin-stimulated cells (Figure 6E). Despite the low amounts of Irs-1 protein present in *Pten* null MEFs, the relative level of tyrosine-phosphorylated Irs-1 was substantial compared to that seen in wild-type MEFs (Figure 6E, compare lanes 2 and 3 with lanes 6 and 7). This enhanced efficiency of Irs-1 tyrosine phosphorylation in *Pten* null cells was no longer apparent after LY294002 treatment, as tyrosine-phosphorylated Irs-1 levels were restored to baseline (Figure 6E, lanes 7 and 8). The kinetics of Irs-1/Ir-β complex assembly was also altered in *Pten* null cells. In both wild-type and *Pten* null MEFs, Ir-β was detected in Irs-1 immunoprecipitates within 5 minutes of insulin stimulation (Figure 6F). After 3 hr, this complex was no longer detectable in wild-type cells but persisted in *Pten* null MEFs (Figure 6F, compare lanes 4 and 9).

Since tyrosine phosphorylation of Irs-1 is thought to preclude serine phosphorylation (Pederson et al., 2001) (and subsequent degradation/inactivation), we propose that the pool of unphosphorylated Irs available for negative feedback regulation is limited in *Pten* null cells.

JUN and AKT Phosphorylation in Human Prostate Cancer Is Positively Correlated

Next we evaluated the relevance of PI3K-driven JNK pathway activation in human cancer by immunohistochemical staining of prostate cancer tissue microarrays (TMAs) for phospho-JUN (pJUN), phosphor-AKT (pAKT), phosphoS6 (pS6), and PTEN. (Figure 7A). pJUN staining was positively correlated with nuclear pAKT (Spearman's Rho = 0.38, $p < 0.0001$) and cytoplasmic pAKT (Spearman's Rho = 0.26, $p = 0.008$) (Figure 7B). pJUN and pS6 were also correlated (Spearman's Rho = 0.57, $p < 0.0001$). There was a trend showing a negative correlation between PTEN expression and pJUN whose strength was comparable to the association between PTEN loss and pAKT or pS6 staining, but neither reached statistical significance. Dual pJUN/PTEN staining with quantum dot-labeled antibodies showed that pJUN and PTEN expression are mutually exclusive in the epithelial cells of prostate tumor sections (Figure 7C). Since AKT phosphorylation is a known marker of *PTEN* loss, the fact that the associations between PTEN loss and pAKT or pJUN failed to reach statistical significance may be indicative of alternative mechanisms of PI3K pathway activation in prostate cancer. The significant positive correlation between pJUN and pAKT suggests that these two molecules are activated by a common upstream signal.

DISCUSSION

Much effort is focused on identifying gene expression networks with the hope that such tools will assist in mining the vast information generated through global expression profiling studies. Gene set enrichment analysis (GSEA) allows detection of modest but coordinated changes in expression of genes involved in a common biological function, rather than concentrating on specific gene changes, and has been successful in elucidating mechanisms of insulin resistance and diabetes (Houstis et al., 2006; Mootha et al., 2003; Petersen et al., 2004; Subramanian et al., 2005). Here we used GSEA to identify pathways associated with PTEN loss using expression data derived from a small number of well-defined isogenic tumor lines (Figure 1A and Figure S7). One lead from this analysis, JNK pathway activation, was then validated in a series of biochemical and biological studies using genetically defined systems. Finally, we demonstrate that the association originally generated from tumor line data sets (through GSEA) is relevant in human clinical samples. Of note, we have conducted further GSEA runs using expression data sets from human prostate cancer samples (http://www.broad.mit.edu/cgi-bin/cancer/publications/pub_paper.cgi?mode=view&paper_id=75) annotated for PTEN status by immunohistochemical staining. The *JNK* pathway gene set also emerged from this analysis, but the strength of the association with PTEN loss was weaker than that found using the isogenic tumor lines (J.R., N.P., and I.V., unpublished data). This presumably reflects the heterogeneity present within human tumor samples and argues for the potential value in starting with genetically defined (albeit artificial systems) for generating initial hypotheses from global data sets then moving to clinical material for validation.

The PTEN/JNK pathway association identified by GSEA was confirmed through a series of biochemical

(B) *Pten*$^{+/+}$ and *Pten*$^{-/-}$ MEF were retrovirally infected with *JunD*-targeted shRNA (JDR). Seventy-two hours after infection, lysates were made and analyzed by immunoblot with the indicated antibodies (bottom). Cells were also seeded and counted as in (A). Growth is expressed as the percentage increase in cell number from day 1 to day 5 in relation to vector-infected cells (100% growth) (left, mean ± SEM, n = 3).
(C) TRAMP-C1 and PTEN-CaP8 cells were retrovirally infected with *Jnk1*-targeted shRNA (J1R). Seventy-two hours after infection, lysates were made and analyzed by immunoblot with the indicated antibodies (bottom). Cells were also seeded and counted as in (A). Growth is expressed as the percentage increase in cell number from day 1 to day 5 in relation to vector-infected cells (100% growth) (left, mean ± SEM, n = 3).
(D) *Pten*$^{+/+}$ and *Pten*$^{-/-}$ MEFs were seeded at equal densities. Fifteen hours after seeding, cells were counted (day 1) and treated with either DMSO (vehicle) or 4 μM JNKi. Cells were counted again 5 days later. Growth is expressed as the percentage increase in cell number from day 1 to day 5 in relation to DMSO-treated cells (100% growth) (left, mean ± SEM, n=3). Cells were also separately treated for 8 hr, as indicated, for biochemical analysis. Lysates were made and examined by immunoblot using the indicated antibodies (middle). c-Jun phosphorylation was quantified by densitometry (right).
(E) *Pten*$^{-/-}$ MEF (control) and *Pten*$^{-/-}$ MEF infected with a *Jnk1*-targeted shRNA (from 3A) were injected subcutaneously into the flanks of SCID mice. Tumor growth was followed and measurements (mean ± SEM) taken at the indicated times.
(F) TRAMP-C1 and PTEN-CaP8 cells were infected with a *Jnk1*-targeted shRNA (J1R). Seventy-two hours after infection, cell lysates were subjected to immunoblot analysis with the indicated antibodies.
(G and H) The remaining cells (from B) were injected subcutaneously into SCID mice (n = 6) and tumor incidence was followed over the indicated time periods.

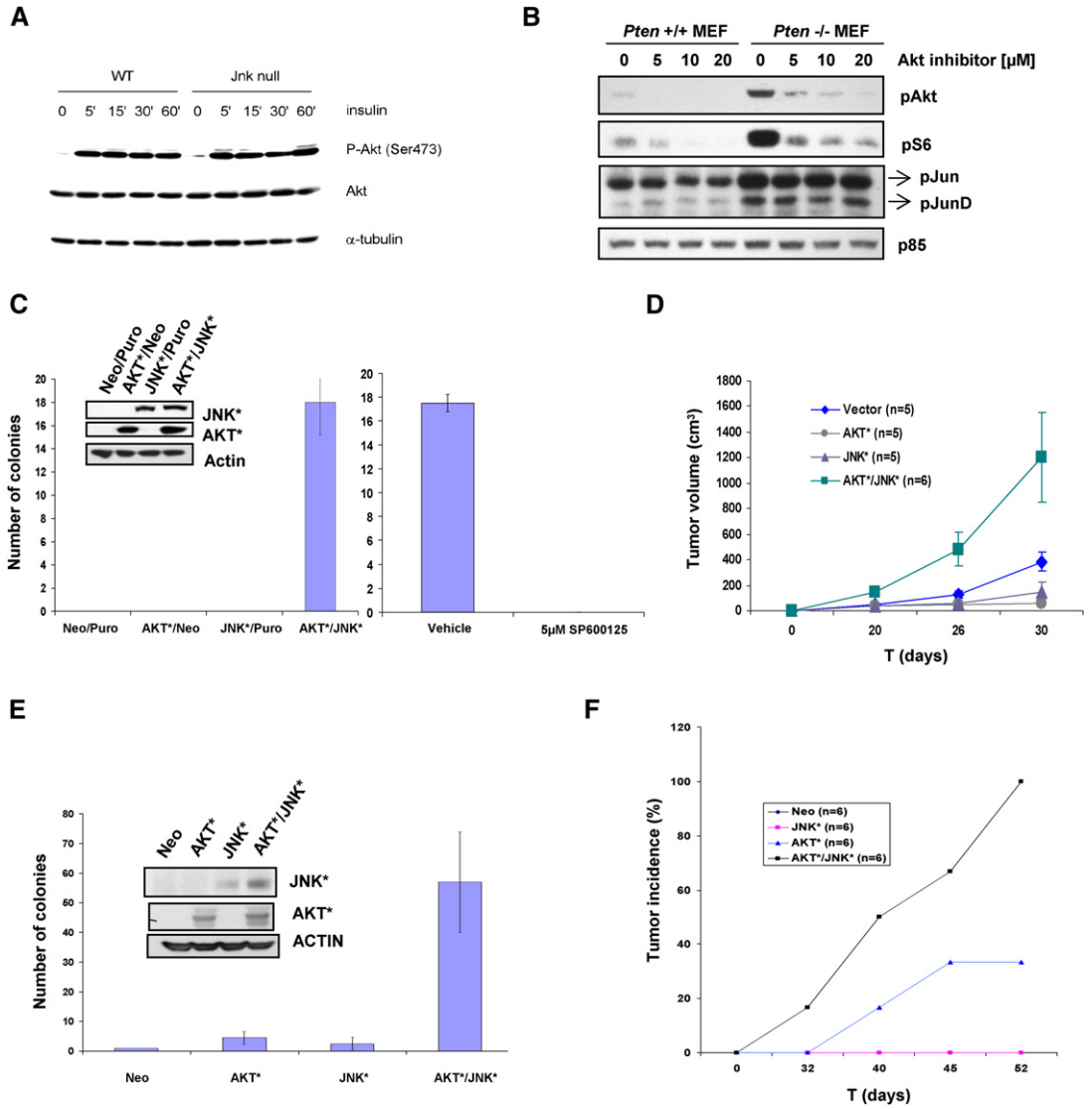

Figure 5. AKT and JNK Are Activated Independently of Each Other and Synergize in Transformation Assays

(A) Wild-type (WT) and *Jnk1/2* double KO (Jnk null) MEFs were serum starved and challenged with 100 nM insulin for the indicated times. Lysates were made and subjected to immunoblot using the indicated antibodies.

(B) Wild-type ($Pten^{+/+}$) and *Pten* null ($Pten^{-/-}$) MEFs were treated with the indicated doses of AKT inhibitor (AKT inhibitor VIII, Calbiochem) for 8 hr. After treatment, cells were lysed and subjected to immunoblot using the indicated antibodies.

(C) NIH3T3 cells were retrovirally transduced with a control virus or viruses carrying constitutively active alleles of epitope-tagged (HA) *AKT* (AKT*), (FLAG) *JNK* (JNK*), or both. Seventy-two hours after infection, cells were lysed and analyzed by western blot using HA (AKT*), FLAG (JNK*), or Actin antibodies (left inset). The remaining cells were plated in soft agar. Colonies were counted three weeks after plating (left bar graph, mean ± SEM, n = 3). A random doubly-transduced clone (AKT*JNK*) from (C) was picked, expanded, and replated in soft agar in the presence or absence of 5 μM SP600125 (right bar graph). Colonies were counted 3 weeks after plating (mean ± SEM, n = 3).

(D) Cells from (C) were injected subcutaneously into SCID mice and tumor volume (mean ± SEM) was measured at the indicated times.

(E) Normal human astrocytes (NHA) were stably transduced with the indicated viruses. Transgene expression was confirmed by western blot analysis using HA (AKT*), FLAG (JNK*), or Actin antibodies (inset). Cells expressing the various transgenes were plated in soft agar. Colonies were counted 3 weeks after plating (mean ± SEM, n = 3).

(F) Astrocytes expressing the indicated transgenes were injected subcutaneously into SCID mice and tumor incidence assessed at the indicated times.

and biological studies using mouse and human cell line models. The evidence includes (1) increased JNK, JUND, and c-JUN phosphorylation (modestly at steady state and significantly after growth factor induction, but not after stress induction) and increased c-Jun transcriptional activity in PTEN null cells and tissues, (2) a synthetic lethal-like dependence of PTEN null cells on JNK1 and JUND for in vitro proliferation and tumor growth, (3)

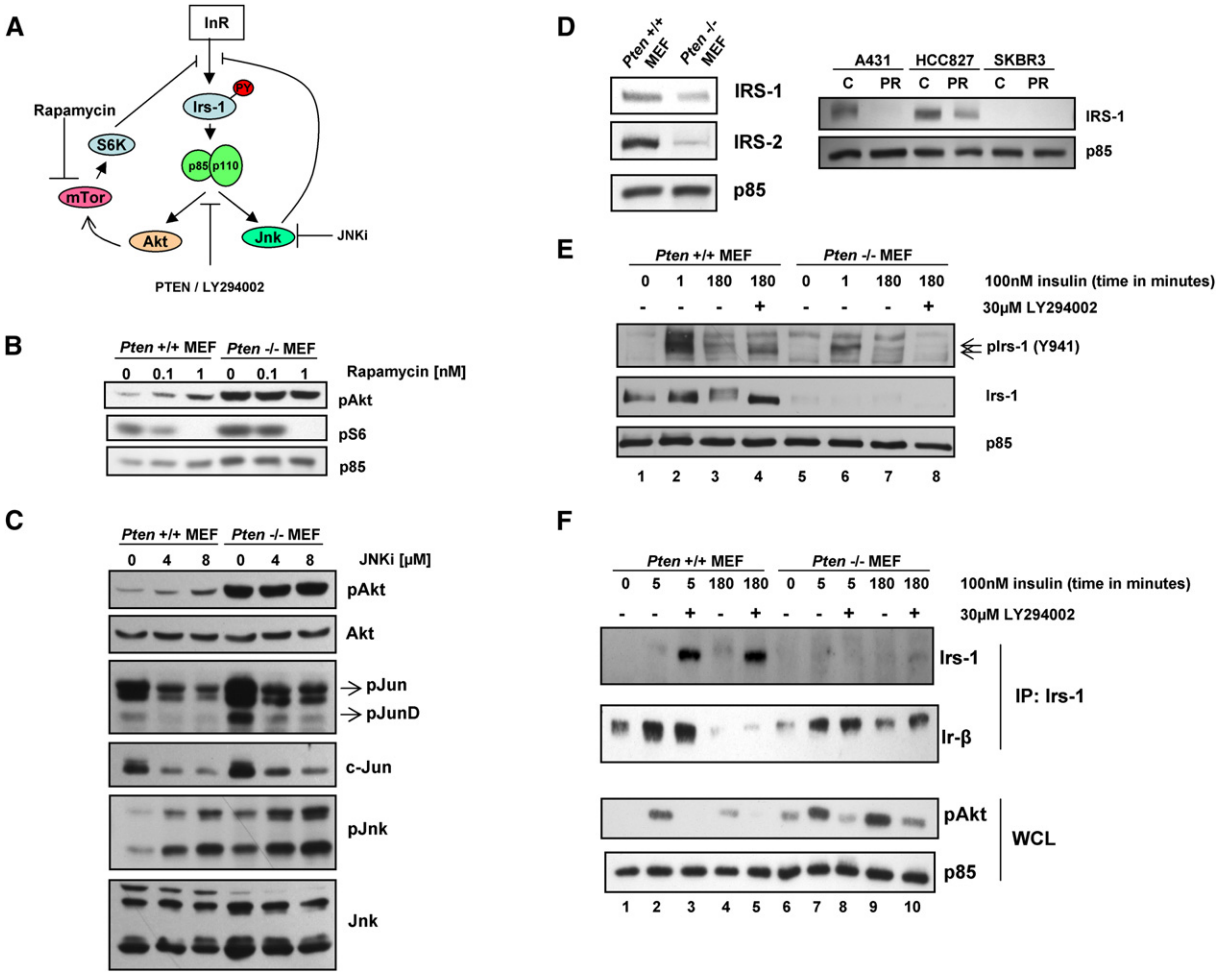

Figure 6. Pi3k Negative Feedback Regulation Is Impaired in *Pten* Null Cells

(A) A model of PI3K negative feedback regulation. Activated insulin receptor phosphorylates IRS-1 at tyrosine residues inducing downstream activation of PI3K. PI3K activates S6K and JNK, both of which phosphorylate IRS-1 at serine residues inducing its degradation and terminating the signal.

(B) *Pten*$^{+/+}$ and *Pten*$^{-/-}$ MEFs were treated with the indicated doses of rapamycin for 8 hr. After treatment, cells were lysed and lysates analyzed by western blot with the indicated antibodies.

(C) *Pten*$^{+/+}$ and *Pten*$^{-/-}$ MEFs were treated for 8 hr with the indicated doses of JNKi. Normalized whole-cell lysates were subjected to western blot analysis with the indicated antibodies.

(D) Irs-1 and Irs-2 protein levels were measured in lysates from *Pten*$^{+/+}$ and *Pten*$^{-/-}$ MEFs by immunoblot. Levels of p85 Pi3k were also measured by western blot for comparison (left). Irs-1 and p85 protein levels were also measured in lysates from the isogenic cell line pairs used for the GSEA as indicated (right).

(E) *Pten*$^{+/+}$ and *Pten*$^{-/-}$ MEFs were serum-starved for 24 hr, then challenged with 100 nM insulin for 1 min or 3 hr and treated with 30 μM LY294002 as indicated. After treatment, lysates were made and analyzed by western blot with the indicated antibodies.

(F) *Pten*$^{+/+}$ and *Pten*$^{-/-}$ MEF cells were serum-starved for 24 hr, then challenged with 100 nM insulin for the indicated times in the presence or absence of 30 μM LY294002. Normalized whole-cell lysates (WCL) were analyzed by western blot using the indicated antibodies or subjected to immunoprecipitation using Irs-1 antibodies. Irs-1 immunoprecipitates were analyzed by western blot using the indicated antibodies.

oncogene cooperativity of JNK with AKT, and (4) association of pJUN and pAKT staining in human prostate cancer specimens. We also show that growth factor-induced JNK activation in *Pten* null cells is Pi3k-dependent via a known pathway involving Rac1 and Mlk3, in agreement with previous observations that Rac1 and Cdc42, two activators in the JNK pathway, exhibited increased catalytic activity in *Pten* null MEFs (Liliental et al., 2000). JNK activation in PTEN null cells is further enhanced by a defect in the termination of JNK signaling, which appears to be mediated through altered transcriptional regulation of downstream target mRNAs. The JNK phosphatases (*DUSP10*, *4*, and *8*) that are downregulated in PTEN null cells are reasonable candidates.

Our studies also shed new light on the mechanism of negative feedback regulation of PI3K, an area of growing

A

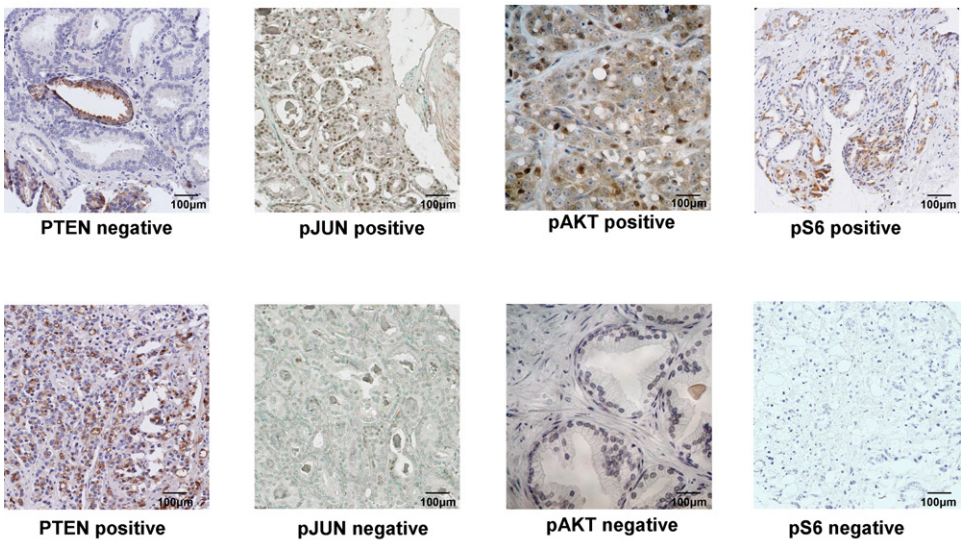

B

Comparison	Number of Tumors	Spearman's Rho	p VALUE
pJUN-nuclear pAKT	98	0.38	<.0001
pJUN-Cytoplasmic pAKT	98	0.26	0.008
pJUN -pS6	100	0.57	<.0001
pS6-nuclear pAKT	98	0.31	0.002
pS6-Cytoplasmic pAKT	98	0.48	<.0001
pJUN -PTEN	98	-0.13	0.194
PTEN-nuclear pAKT	97	-0.15	0.1433
PTEN-Cytoplasmic pAKT	97	-0.05	0.5964
pS6- PTEN	98	-0.11	0.29

C

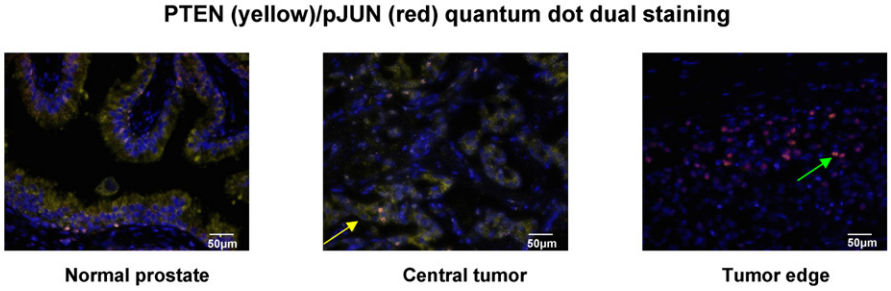

Figure 7. Phospho-JUN and Phospho-AKT Immunohistochemical Staining Are Positively Correlated in Human Clinical Prostate Cancer Samples

(A) Representative images from prostate cancer tissue microarrays stained with PTEN, pJUN, pAKT, and pS6 antibodies.

(B) Relationship between pJUN, pAKT, pS6, and PTEN staining scores from tumor tissue microarray samples using the Spearman correlation coefficient.

(C) Dual PTEN (yellow) and pJUN (red) quantum-dot-labeled antibody staining of normal prostate and prostate cancer samples. The yellow arrow points to PTEN positive cells. The green arrow points to pJUN-positive cells.

interest due to the clinical use of mTOR inhibitors as anticancer agents. These drugs can activate AKT in some tumors due to loss of S6 kinase-mediated negative feedback, potentially counteracting their intended anticancer activity. IRS proteins, which function primarily (upon tyrosine phosphorylation) to activate PI3K, are also the targets of the S6 kinase and JNK negative feedback loop (through serine phosphorylation). Our data demonstrate that IRS proteins in *Pten* null cells, which are limited due to reduced mRNA levels, are more efficiently phosphorylated on tyrosine and engaged in signal transduction due to sustained complex formation with Ir-β. We propose that this prolonged pattern of Irs tyrosine phosphorylation and Ir-β complex formation limits the

pool available for serine phosphorylation by S6 kinase or Jnk, thereby impairing negative feedback. The precise mechanism by which PTEN loss alters IRS function needs further exploration. One possibility is that sustained levels of PIP_3 caused by PTEN loss recruit IRS proteins to the membrane through interaction with their PH domains (Razzini et al., 2000; Voliovitch et al., 1995) and thereby gain greater proximity to tyrosine phosphorylation by receptor tyrosine kinases.

The cooperativity between AKT and JNK in transformation models is particularly relevant for therapeutics since small molecule inhibitors of both targets are in clinical development. JNK is known to promote apoptosis in certain contexts, yet the proapoptotic effects of JNK are suppressed by PI3K-driven signals (Lamb et al., 2003; Lei et al., 2002; Xia et al., 1995). One might predict, then, that AKT inhibition alone could unleash the proapoptotic activity of JNK in PTEN null cells, whereas parallel inhibition of JNK and AKT may be counterproductive. However, we found that proliferation, and particularly tumor formation, of PTEN null cells is suppressed by JNK1 inhibition, analogous to the role of JNK1 in leukemic spread in a murine BCR-ABL leukemia model (Hess et al., 2002). This dual role of JNK1 is similar to that observed for JUND (also implicated in our studies), which shifts from tumor suppressor to oncogene in the context of MEN1 deletion (Agarwal et al., 2003). Therefore, dual inhibition of AKT and JNK may be appropriate only in the context of *PTEN* loss. Notably, somatic mutations in *JNK1*, *JNK2*, and the upstream kinase *MKK7* were recently reported in human tumors, providing further evidence of a role for this pathway in transformation (Greenman et al., 2007). As inhibitors of AKT, JNK, PI3K, mTOR, and the insulin and IGF receptor tyrosine kinases all make their way into the clinic, our findings reinforce the need to document tumor genotype to make an informed assessment of clinical response.

EXPERIMENTAL PROCEDURES

GSEA Analysis

The human isogenic cell line pairs were profiled using Affymetrix Human Genome U133 Plus 2.0 Arrays in duplicate. The data were restricted to only those probes that were flagged as present in 1 out of 4 samples. GSEA was performed using the publicly available desktop application from the Broad Institute (http://www.broad.mit.edu/gsea/software/software_index.html). Genes represented by more than one probe were collapsed using the XCollapseProbes utility to the probe with the maximum value. The gene sets database used was that of functional sets, s2.symbols.gmt. Due to the small number of samples, p values were calculated by permuting the genes 1000 times. The classic enrichment statistic was selected. The HG-U95Av2 clinical prostate cancer data set was restricted by rejecting 10% of the probes: those with the lowest signal intensity. This was done by removing genes with signal lower than seven in 3 of 13 conditions. The same procedure was repeated for GSEA.

Microarray Data Access

All microarray data from the isogenic cell line pairs used for GSEA have been deposited in NCBIs Gene Expression Omnibus (GEO, http://www.ncbi.nlm.nih.gov/geo/) and are accessible through GEO series accession number GSE7562.

Cell Culture and Agar Assays

MEFs and NIH-3T3 cells were grown in DMEM supplemented with 5% fetal bovine serum (FBS). Normal human astrocytes (NHA) (gift from Dr. Russell Pieper) were grown in DMEM supplemented with 10% FBS. To generate $Pten^{-/-}$ MEFs, Cre recombinase virus was made by transfecting pMSCV-puro-Cre and ecotropic packaging plasmid into 293T cells. Virus was collected and $Pten^{lox/lox}$ MEFs were infected. Cells were selected with 3 ug/ml puromycin for 5 days. *Jnk1* and *Jnk2* shRNA as well as constitutively active AKT (AKT*) and constitutively active JNK (JNK*) ecotropic retroviruses were also made in this manner, but the analysis was done 72 hr after infection. To generate NHA cells expressing vector control, JNK*, AKT* or JNK*, and AKT*, viruses were generated by transfecting pMSCV-Neo, JNK* or AKT* into an amphotropic packaging cell line. Cells were infected and stable expressors were selected by adding 500 ug/ml G418, or 3 ug/ml puromycin into the media for 10 days. JNK*/AKT* double expressors were generated by retrovirally introducing JNK* into NHA-AKT* cells and selecting with G418 for 10 days. Soft agar assays were done as previously described (Li et al., 1995).

In Vivo Tumor Growth

All animal experiments were approved by the UCLA Animal Research committee and conducted according to relevant regulatory standards. 1×10^6 cells resuspended in 50% matrigel were injected into the flanks of SCID mice. Growth was followed over time by taking caliper measurements at the indicated times.

Protein Expression Analysis

Irs-1 immunoprecipitations were carried out for 3 hr at 4°C. Immunoprecipitates were eluted by boiling samples in 3% SDS for 5 min. Reporter assays of Jnk activity were done using the PathDetect c-Jun Trans-reporting System (Stratagene). Cells were transfected using Lipofectamine 2000 (Invitrogen). Dominant negative *MLK3* (pCDNA-MLK3-K144R) was a gift from Dr. Norman Lassam. Dominant negative *RAC1* (pCDNA-Rac1-N17) was a gift from Dr. David Chang. Constitutively active p110-α (pCG-M-p110*) was a gift from Dr. Anke Klippel. Transfected cells were lysed and luciferase assays carried out using the Dual-Luciferase Reporter Assay System (Promega).

Immunohistochemical and Quantum Dot Staining and Analysis

Tissue acquisition for making prostate tissue microarrays was performed under an approved protocol from the Dana Farber Cancer Institute Institutional Review Board (IRB99-33). Informed consent for these studies was received from patients under the terms of IRB 01-145. Immunohistochemistry (IHC) was performed on 5 μm thick, formalin-fixed, paraffin-embedded TMA sections using primary antibodies for PTEN (1:200 dilution, 60 min at room temperature incubation, Zymed Laboratories, San Francisco, CA), phospho cJUN Ser 73 (1:50 dilution, overnight 4°C incubation, Cell Signaling Technology, Danvers, MA), phospho S6 Ser 240/244, (1:100 dilution, overnight 4°C incubation, Cell Signaling Technology, Danvers, MA), and pAKT (Ser 473) (Cell Signaling Technology, Danvers, MA, 1:50 dilution, overnight 4°C incubation). Antigen retrieval was performed for 30 min in citrate buffer for each antibody, except pAKT where three 5 min cycles in citrate buffer was used. A BioGenex I 6000 autostainer was used for all subsequent steps (BioGenex, San Ramon, CA). Secondary antibody and DAB disclosure was used for conventional IHC. In the case of dual quantum dot disclosed immunohistochemistry, Qdot 605 and Qdot 650 (Invitrogen, Carlsbad, CA) were used sequentially with intervening blocking steps for disclosure of Phospho c-Jun and PTEN respectively. Duplex Quantum dot signals were deconvoluted using the Nuance Multispectral Imager (CRI Inc., Cambridge, MA). TMAs were scored semiquantitatively using an Intensity X Quantity product: (Intensity: 0 = Negative, 1 = Weak, 2 = Moderate, 3 = Strong; Quantity: 0 = Negative, 1 = 1%–9% of examined cells positive, 2 = 10%–39% of cells positive, 3 = 40%–69% of cells positive, 4 = 70%–100% of cells positive). Scores were averaged across replicate cores.

Supplemental Data

The Supplemental Data include seven supplemental figures, one supplemental table, and supplemental experimental procedures and can be found with this article online at http://www.cancercell.org/cgi/content/full/11/6/555/DC1/.

ACKNOWLEDGMENTS

C.L.S. is a Doris Duke Distinguished Clinical Scientist and a former Investigator of the Howard Hughes Medical Institute. This work was supported by grants from the US National Cancer Institute and the UCLA Prostate SPORE seed grant. I.V. was also supported by a Ruth L. Kirschstein National Research Service Award (5F31GM067600). We would like to thank Andrew Kwon and Teli Hsueh for technical assistance and George Thomas for help with the scoring of PTEN immunohistochemical stains.

Received: August 11, 2006
Revised: February 14, 2007
Accepted: April 30, 2007
Published: June 11, 2007

REFERENCES

Agarwal, S.K., Novotny, E.A., Crabtree, J.S., Weitzman, J.B., Yaniv, M., Burns, A.L., Chandrasekharappa, S.C., Collins, F.S., Spiegel, A.M., and Marx, S.J. (2003). Transcription factor JunD, deprived of menin, switches from growth suppressor to growth promoter. Proc. Natl. Acad. Sci. USA *100*, 10770–10775.

Angel, P., Hattori, K., Smeal, T., and Karin, M. (1988). The jun proto-oncogene is positively autoregulated by its product, Jun/AP-1. Cell *55*, 875–885.

Antonyak, M.A., Kenyon, L.C., Godwin, A.K., James, D.C., Emlet, D.R., Okamoto, I., Tnani, M., Holgado-Madruga, M., Moscatello, D.K., and Wong, A.J. (2002). Elevated JNK activation contributes to the pathogenesis of human brain tumors. Oncogene *21*, 5038–5046.

Barnett, S.F., Defeo-Jones, D., Fu, S., Hancock, P.J., Haskell, K.M., Jones, R.E., Kahana, J.A., Kral, A.M., Leander, K., Lee, L.L., et al. (2005). Identification and characterization of pleckstrin-homology-domain-dependent and isoenzyme-specific Akt inhibitors. Biochem. J. *385*, 399–408.

Davis, R.J. (2000). Signal transduction by the JNK group of MAP kinases. Cell *103*, 239–252.

Dickens, M., Rogers, J.S., Cavanagh, J., Raitano, A., Xia, Z., Halpern, J.R., Greenberg, M.E., Sawyers, C.L., and Davis, R.J. (1997). A cytoplasmic inhibitor of the JNK signal transduction pathway. Science *277*, 693–696.

Du, L., Lyle, C.S., Obey, T.B., Gaarde, W.A., Muir, J.A., Bennett, B.L., and Chambers, T.C. (2004). Inhibition of cell proliferation and cell cycle progression by specific inhibition of basal JNK activity: Evidence that mitotic Bcl-2 phosphorylation is JNK-independent. J. Biol. Chem. *279*, 11957–11966.

Easton, J.B., Kurmasheva, R.T., and Houghton, P.J. (2006). IRS-1: Auditing the effectiveness of mTOR inhibitors. Cancer Cell *9*, 153–155.

Foster, B.A., Gingrich, J.R., Kwon, E.D., Madias, C., and Greenberg, N.M. (1997). Characterization of prostatic epithelial cell lines derived from transgenic adenocarcinoma of the mouse prostate (TRAMP) model. Cancer Res. *57*, 3325–3330.

Freeman, D.J., Li, A.G., Wei, G., Li, H.H., Kertesz, N., Lesche, R., Whale, A.D., Martinez-Diaz, H., Rozengurt, N., Cardiff, R.D., et al. (2003). PTEN tumor suppressor regulates p53 protein levels and activity through phosphatase-dependent and -independent mechanisms. Cancer Cell *3*, 117–130.

Fujishiro, M., Gotoh, Y., Katagiri, H., Sakoda, H., Ogihara, T., Anai, M., Onishi, Y., Ono, H., Abe, M., Shojima, N., et al. (2003). Three mitogen-activated protein kinases inhibit insulin signaling by different mechanisms in 3T3–L1 adipocytes. Mol. Endocrinol. *17*, 487–497.

Greenman, C., Stephens, P., Smith, R., Dalgliesh, G.L., Hunter, C., Bignell, G., Davies, H., Teague, J., Butler, A., Stevens, C., et al. (2007). Patterns of somatic mutation in human cancer genomes. Nature *446*, 153–158.

Groszer, M., Erickson, R., Scripture-Adams, D.D., Dougherty, J.D., Le Belle, J., Zack, J.A., Geschwind, D.H., Liu, X., Kornblum, H.I., and Wu, H. (2006). PTEN negatively regulates neural stem cell self-renewal by modulating G0–G1 cell cycle entry. Proc. Natl. Acad. Sci. USA *103*, 111–116.

Gual, P., Le Marchand-Brustel, Y., and Tanti, J.F. (2005). Positive and negative regulation of insulin signaling through IRS-1 phosphorylation. Biochimie *87*, 99–109.

Haruta, T., Uno, T., Kawahara, J., Takano, A., Egawa, K., Sharma, P.M., Olefsky, J.M., and Kobayashi, M. (2000). A rapamycin-sensitive pathway down-regulates insulin signaling via phosphorylation and proteasomal degradation of insulin receptor substrate-1. Mol. Endocrinol. *14*, 783–794.

Hess, P., Pihan, G., Sawyers, C.L., Flavell, R.A., and Davis, R.J. (2002). Survival signaling mediated by c-Jun NH(2)-terminal kinase in transformed B lymphoblasts. Nat. Genet. *32*, 201–205.

Hirosumi, J., Tuncman, G., Chang, L., Gorgun, C.Z., Uysal, K.T., Maeda, K., Karin, M., and Hotamisligil, G.S. (2002). A central role for JNK in obesity and insulin resistance. Nature *420*, 333–336.

Hong, T.M., Yang, P.C., Peck, K., Chen, J.J., Yang, S.C., Chen, Y.C., and Wu, C.W. (2000). Profiling the downstream genes of tumor suppressor PTEN in lung cancer cells by complementary DNA microarray. Am. J. Respir. Cell Mol. Biol. *23*, 355–363.

Houstis, N., Rosen, E.D., and Lander, E.S. (2006). Reactive oxygen species have a causal role in multiple forms of insulin resistance. Nature *440*, 944–948.

Inoki, K., Li, Y., Zhu, T., Wu, J., and Guan, K.L. (2002). TSC2 is phosphorylated and inhibited by Akt and suppresses mTOR signalling. Nat. Cell Biol. *4*, 648–657.

Kiger, A.A., Baum, B., Jones, S., Jones, M.R., Coulson, A., Echeverri, C., and Perrimon, N. (2003). A functional genomic analysis of cell morphology using RNA interference. J. Biol. *2*, 27.

Klippel, A., Reinhard, C., Kavanaugh, W.M., Apell, G., Escobedo, M.A., and Williams, L.T. (1996). Membrane localization of phosphatidylinositol 3-kinase is sufficient to activate multiple signal-transducing kinase pathways. Mol. Cell. Biol. *16*, 4117–4127.

Lamb, J.A., Ventura, J.J., Hess, P., Flavell, R.A., and Davis, R.J. (2003). JunD mediates survival signaling by the JNK signal transduction pathway. Mol. Cell *11*, 1479–1489.

Lee, Y.H., Giraud, J., Davis, R.J., and White, M.F. (2003). c-Jun N-terminal kinase (JNK) mediates feedback inhibition of the insulin signaling cascade. J. Biol. Chem. *278*, 2896–2902.

Lei, K., Nimnual, A., Zong, W.X., Kennedy, N.J., Flavell, R.A., Thompson, C.B., Bar-Sagi, D., and Davis, R.J. (2002). The Bax subfamily of Bcl2-related proteins is essential for apoptotic signal transduction by c-Jun NH(2)-terminal kinase. Mol. Cell. Biol. *22*, 4929–4942.

Li, G., Hu, Y., Huo, Y., Liu, M., Freeman, D., Gao, J., Liu, X., Wu, D., and Wu, H. (2006). PTEN deletion leads to up-regulation of a secreted growth factor pleiotrophin. J. Biol Chem. *281*, 10663–10668.

Li, T., Tsukada, S., Satterthwaite, A., Havlik, M.H., Park, H., Takatsu, K., and Witte, O.N. (1995). Activation of Bruton's tyrosine kinase (BTK) by a point mutation in its pleckstrin homology (PH) domain. Immunity *2*, 451–460.

Liliental, J., Moon, S.Y., Lesche, R., Mamillapalli, R., Li, D., Zheng, Y., Sun, H., and Wu, H. (2000). Genetic deletion of the Pten tumor suppressor gene promotes cell motility by activation of Rac1 and Cdc42 GTPases. Curr. Biol. *10*, 401–404.

Majumder, P.K., Febbo, P.G., Bikoff, R., Berger, R., Xue, Q., McMahon, L.M., Manola, J., Brugarolas, J., McDonnell, T.J., Golub, T.R., et al. (2004). mTOR inhibition reverses Akt-dependent prostate

intraepithelial neoplasia through regulation of apoptotic and HIF-1-dependent pathways. Nat. Med. *10*, 594–601.

Majumder, P.K., Yeh, J.J., George, D.J., Febbo, P.G., Kum, J., Xue, Q., Bikoff, R., Ma, H., Kantoff, P.W., Golub, T.R., et al. (2003). Prostate intraepithelial neoplasia induced by prostate restricted Akt activation: The MPAKT model. Proc. Natl. Acad. Sci. USA *100*, 7841–7846.

Manning, A.M., and Davis, R.J. (2003). Targeting JNK for therapeutic benefit: From junk to gold? Nat. Rev. Drug Discov. *2*, 554–565.

Monti, S., Savage, K.J., Kutok, J.L., Feuerhake, F., Kurtin, P., Mihm, M., Wu, B., Pasqualucci, L., Neuberg, D., Aguiar, R.C., et al. (2005). Molecular profiling of diffuse large B-cell lymphoma identifies robust subtypes including one characterized by host inflammatory response. Blood *105*, 1851–1861.

Mootha, V.K., Lindgren, C.M., Eriksson, K.F., Subramanian, A., Sihag, S., Lehar, J., Puigserver, P., Carlsson, E., Ridderstrale, M., Laurila, E., et al. (2003). PGC-1alpha-responsive genes involved in oxidative phosphorylation are coordinately downregulated in human diabetes. Nat. Genet. *34*, 267–273.

Musatov, S., Roberts, J., Brooks, A.I., Pena, J., Betchen, S., Pfaff, D.W., and Kaplitt, M.G. (2004). Inhibition of neuronal phenotype by PTEN in PC12 cells. Proc. Natl. Acad. Sci. USA *101*, 3627–3631.

Neshat, M.S., Mellinghoff, I.K., Tran, C., Stiles, B., Thomas, G., Petersen, R., Frost, P., Gibbons, J.J., Wu, H., and Sawyers, C.L. (2001). Enhanced sensitivity of PTEN-deficient tumors to inhibition of FRAP/mTOR. Proc. Natl. Acad. Sci. USA *98*, 10314–10319.

O'Reilly, K.E., Rojo, F., She, Q.B., Solit, D., Mills, G.B., Smith, D., Lane, H., Hofmann, F., Hicklin, D.J., Ludwig, D.L., et al. (2006). mTOR inhibition induces upstream receptor tyrosine kinase signaling and activates Akt. Cancer Res. *66*, 1500–1508.

Pederson, T.M., Kramer, D.L., and Rondinone, C.M. (2001). Serine/threonine phosphorylation of IRS-1 triggers its degradation: Possible regulation by tyrosine phosphorylation. Diabetes *50*, 24–31.

Petersen, K.F., Dufour, S., Befroy, D., Garcia, R., and Shulman, G.I. (2004). Impaired mitochondrial activity in the insulin-resistant offspring of patients with type 2 diabetes. N. Engl. J. Med. *350*, 664–671.

Pfarr, C.M., Mechta, F., Spyrou, G., Lallemand, D., Carillo, S., and Yaniv, M. (1994). Mouse JunD negatively regulates fibroblast growth and antagonizes transformation by ras. Cell *76*, 747–760.

Podsypanina, K., Lee, R.T., Politis, C., Hennessy, I., Crane, A., Puc, J., Neshat, M., Wang, H., Yang, L., Gibbons, J., et al. (2001). An inhibitor of mTOR reduces neoplasia and normalizes p70/S6 kinase activity in Pten+/− mice. Proc. Natl. Acad. Sci. USA *98*, 10320–10325.

Raitano, A.B., Halpern, J.R., Hambuch, T.M., and Sawyers, C.L. (1995). The Bcr-Abl leukemia oncogene activates Jun kinase and requires Jun for transformation. Proc. Natl. Acad. Sci. USA *92*, 11746–11750.

Razzini, G., Ingrosso, A., Brancaccio, A., Sciacchitano, S., Esposito, D.L., and Falasca, M. (2000). Different subcellular localization and phosphoinositides binding of insulin receptor substrate protein pleckstrin homology domains. Mol. Endocrinol. *14*, 823–836.

Rodrigues, G.A., Park, M., and Schlessinger, J. (1997). Activation of the JNK pathway is essential for transformation by the Met oncogene. EMBO J. *16*, 2634–2645.

Shi, Y., Yan, H., Frost, P., Gera, J., and Lichtenstein, A. (2005). Mammalian target of rapamycin inhibitors activate the AKT kinase in multiple myeloma cells by up-regulating the insulin-like growth factor receptor/insulin receptor substrate-1/phosphatidylinositol 3-kinase cascade. Mol. Cancer Ther. *4*, 1533–1540.

Simpson, L., Li, J., Liaw, D., Hennessy, I., Oliner, J., Christians, F., and Parsons, R. (2001). PTEN expression causes feedback upregulation of insulin receptor substrate 2. Mol. Cell. Biol. *21*, 3947–3958.

Sonoda, Y., Ozawa, T., Aldape, K.D., Deen, D.F., Berger, M.S., and Pieper, R.O. (2001). Akt pathway activation converts anaplastic astrocytoma to glioblastoma multiforme in a human astrocyte model of glioma. Cancer Res. *61*, 6674–6678.

Stolarov, J., Chang, K., Reiner, A., Rodgers, L., Hannon, G.J., Wigler, M.H., and Mittal, V. (2001). Design of a retroviral-mediated ecdysone-inducible system and its application to the expression profiling of the PTEN tumor suppressor. Proc. Natl. Acad. Sci. USA *98*, 13043–13048.

Subramanian, A., Tamayo, P., Mootha, V.K., Mukherjee, S., Ebert, B.L., Gillette, M.A., Paulovich, A., Pomeroy, S.L., Golub, T.R., Lander, E.S., and Mesirov, J.P. (2005). Gene set enrichment analysis: A knowledge-based approach for interpreting genome-wide expression profiles. Proc. Natl. Acad. Sci. USA *102*, 15545–15550.

Sun, S.Y., Rosenberg, L.M., Wang, X., Zhou, Z., Yue, P., Fu, H., and Khuri, F.R. (2005). Activation of Akt and eIF4E survival pathways by rapamycin-mediated mammalian target of rapamycin inhibition. Cancer Res. *65*, 7052–7058.

Szczepankiewicz, B.G., Kosogof, C., Nelson, L.T., Liu, G., Liu, B., Zhao, H., Serby, M.D., Xin, Z., Liu, M., Gum, R.J., et al. (2006). Aminopyridine-based c-Jun N-terminal kinase inhibitors with cellular activity and minimal cross-kinase activity. J. Med. Chem. *49*, 3563–3580.

Trotman, L.C., Niki, M., Dotan, Z.A., Koutcher, J.A., Di Cristofano, A., Xiao, A., Khoo, A.S., Roy-Burman, P., Greenberg, N.M., Van Dyke, T., et al. (2003). Pten dose dictates cancer progression in the prostate. PLoS Biol. *1*, E59. 10.1371/journal.pbio.0000059.

Vivanco, I., and Sawyers, C.L. (2002). The phosphatidylinositol 3-Kinase AKT pathway in human cancer. Nat. Rev. Cancer *2*, 489–501.

Voliovitch, H., Schindler, D.G., Hadari, Y.R., Taylor, S.I., Accili, D., and Zick, Y. (1995). Tyrosine phosphorylation of insulin receptor substrate-1 in vivo depends upon the presence of its pleckstrin homology region. J. Biol. Chem. *270*, 18083–18087.

Wang, S., Gao, J., Lei, Q., Rozengurt, N., Pritchard, C., Jiao, J., Thomas, G.V., Li, G., Roy-Burman, P., Nelson, P.S., et al. (2003). Prostate-specific deletion of the murine Pten tumor suppressor gene leads to metastatic prostate cancer. Cancer Cell *4*, 209–221.

Wang, S.I., Puc, J., Li, J., Bruce, J.N., Cairns, P., Sidransky, D., and Parsons, R. (1997). Somatic mutations of PTEN in glioblastoma multiforme. Cancer Res. *57*, 4183–4186.

Wendel, H.G., De Stanchina, E., Fridman, J.S., Malina, A., Ray, S., Kogan, S., Cordon-Cardo, C., Pelletier, J., and Lowe, S.W. (2004). Survival signalling by Akt and eIF4E in oncogenesis and cancer therapy. Nature *428*, 332–337.

Wolter, S., Mushinski, J.F., Saboori, A.M., Resch, K., and Kracht, M. (2002). Inducible expression of a constitutively active mutant of mitogen-activated protein kinase kinase 7 specifically activates c-JUN NH2-terminal protein kinase, alters expression of at least nine genes, and inhibits cell proliferation. J. Biol. Chem. *277*, 3576–3584.

Xia, Z., Dickens, M., Raingeaud, J., Davis, R.J., and Greenberg, M.E. (1995). Opposing effects of ERK and JNK-p38 MAP kinases on apoptosis. Science *270*, 1326–1331.

Yilmaz, O.H., Valdez, R., Theisen, B.K., Guo, W., Ferguson, D.O., Wu, H., and Morrison, S.J. (2006). Pten dependence distinguishes haematopoietic stem cells from leukaemia-initiating cells. Nature *441*, 475–482.

Zhao, J.J., Gjoerup, O.V., Subramanian, R.R., Cheng, Y., Chen, W., Roberts, T.M., and Hahn, W.C. (2003). Human mammary epithelial cell transformation through the activation of phosphatidylinositol 3-kinase. Cancer Cell *3*, 483–495.

Zhao, Z., Leister, W.H., Robinson, R.G., Barnett, S.F., Defeo-Jones, D., Jones, R.E., Hartman, G.D., Huff, J.R., Huber, H.E., Duggan, M.E., and Lindsley, C.W. (2005). Discovery of 2,3,5-trisubstituted pyridine derivatives as potent Akt1 and Akt2 dual inhibitors. Bioorg. Med. Chem. Lett. *15*, 905–909.

Accession Numbers

All microarray data from the isogenic cell line pairs used for GSEA have been deposited in NCBIs Gene Expression Omnibus (GEO, http://www.ncbi.nlm.nih.gov/geo/) and are accessible through GEO series accession number GSE7562.